Proceedings of the 21st ICSMGE, Vienna, Austria, 14 – 19 June 2026. Pistrol, Adam & Schweiger (eds.)
Published by: ÖGG, Austrian Society for Geomechanics, Salzburg, Austria, ISBN 978-3-9503898-4-5
https://doi.org/10.53243/ICSMGE2026-827

Comparative Assessment of Damping Models for Small-Strain Ground Response Analysis: A Case Study at the Delaney Park Downhole Array site

Nishkarsha Dawadi, Brady R. Cox
Department of Civil and Environmental Engineering, Utah State University, USA, nishkarsha.dawadi@usu.edu

Kami Mohammadi
Department of Civil and Environmental Engineering, University of Utah, USA

Mohamad M. Hallal
Department of Civil and Environmental Engineering, University of California, Berkeley, USA

ABSTRACT: Recent studies have shown that accurately predicting small-strain seismic site response at the Delaney Park Downhole Array (DPDA) site in Anchorage, Alaska, is challenging due to consistent overestimation of empirical transfer function (ETF) amplification peaks. Some researchers have attempted to improve theoretical transfer function (TTF) predictions by increasing the small-strain damping ratio (D_{min}) as a means to reduce amplification, though these efforts have largely been confined to one-dimensional (1D) analyses. While increasing D_{min} improves agreement between TTF and ETF at the fundamental mode peak, it often leads to substantial underprediction of ETF at higher mode peaks. This study evaluates the effectiveness of three numerical damping formulations anchored at two different small-strain damping ratios in modeling seismic site response at DPDA site using a two-dimensional (2D) numerical ground response analysis (GRA) framework. Linear-viscoelastic 2D GRAs were implemented to capture the site's spatial variability while avoiding complexities from modeling nonlinear soil behavior. Numerical analyses were conducted in FLAC-3D using the most heterogeneous cross-section extracted from a pseudo-3D shear wave velocity (Vs) model of the DPDA site. The damping formulations evaluated include Full Rayleigh, Maxwell ("frequency-independent"), and Rayleigh Mass, each implemented with both the conventional D_{min} and a modified damping ratio ($8 \times D_{min}$) derived through site-specific calibration. TTFs from each case were compared with ETFs computed from 56 recorded weak ground motions. Results show that Rayleigh Mass damping with the modified damping ratio provides the best agreement with the observed site response, reducing transfer function misfit by 42% relative to Full Rayleigh and 50% relative to Maxwell over the frequency range of interest. Rayleigh Mass damping also achieved analysis times 14 times faster than Full Rayleigh and 1.7 times faster than Maxwell. Its strong performance, despite inherent frequency dependence, suggests revisiting the prevailing preference for frequency-independent damping in site response modeling.

KEYWORDS: Site Response, Ground Response Analysis, Damping, Delaney Park Downhole Array

1 INTRODUCTION

Ground response analyses (GRAs) examine how seismic waves are altered in amplitude, frequency content, and duration as they propagate from the bedrock through overlying soil layers to the ground surface. GRAs play a vital role in seismic hazard assessment and critical infrastructure design. While one-dimensional (1D) GRAs are common in engineering practice due to their simplicity and computational efficiency, they fail to capture the complexity introduced by lateral heterogeneity in subsurface materials. This simplification can lead to misrepresentation of attenuation mechanisms such as wave scattering, particularly in regions with significant spatial variability. Recent studies at borehole array sites have shown that, on average, more than 50% of the sites are poorly modeled using 1D GRAs (Hallal et al., 2022). Furthermore, 1D GRA studies carried out at downhole array sites (e.g., Afshari & Stewart, 2019; Tao & Rathje, 2019; Hallal & Cox, 2021b) have found that there is a consistent overprediction of the fundamental mode frequency peak. This persistent overprediction of the fundamental mode frequency peak can be attributed to the fact that traditional laboratory-derived damping values typically capture only material damping and do not account for additional energy losses associated with wave scattering and complex wavefield interactions in the field. To address this, some researchers have implemented modified damping (e.g., Tsai & Hashash, 2009; Tao & Rathje, 2019). While these damping adjustments helped reduce the overestimation at the fundamental-mode peak, they often led to an underprediction of amplification at higher mode frequencies (Hallal et al., 2022).

Advances in computational modeling have enabled more realistic two-dimensional (2D) and three-dimensional (3D) GRAs, which can account for non-vertical wave propagation and wave scattering. However, the lack of large-scale, site-specific, multi-dimensional subsurface models that accurately represent laterally varying material properties, such as shear wave velocity (Vs) and material damping, has limited the widespread adoption of 2D and 3D GRAs. Only a few studies have implemented multi-dimensional GRAs at downhole array sites, including 2D GRA at the Treasure Island Downhole Array (TIDA) site (Hallal & Cox, 2023), 2D GRA at the Delaney Park Downhole Array (DPDA) site (Dawadi et al., 2024), and 3D GRA at the I-15 Downhole Array (I15DA) site (Dawadi et al., 2025). Each of these analyses was conducted using pseudo-3D Vs models developed via the horizontal-to-vertical spectral ratio (H/V) geostatistical approach proposed by Hallal & Cox (2021a). These studies collectively found that the presence of undulations and secondary peaks in the simulated theoretical transfer functions (TTFs) indicated that multi-dimensional GRAs improved the ability to capture spatial variability at each site. However, comparison of the TTFs with recorded small-strain empirical transfer functions (ETFs) showed that accounting for spatial variability through 2D/3D GRAs alone did not resolve the significant overestimation of the amplitude at the fundamental frequency, a persistent issue also observed in TTFs obtained from 1D GRAs.

In this study, we conduct 2D GRA at the DPDA site in Anchorage, Alaska, using a pseudo-3D Vs and damping model developed using the H/V geostatistical approach. We evaluate three numerical damping formulations: (1) Full Rayleigh damping, (2) Maxwell damping, and (3) Rayleigh Mass damping. Each damping formulation is applied in combination with the conventional small-strain damping ratio (D_{min}) and a modified damping ratio ($8 \times D_{min}$) derived from site-specific calibration. Analyses are conducted in FLAC-3D (Itasca Consulting Group, 2023), and the TTFs obtained from each analysis are compared to the median ETF computed from 56 recorded weak ground motions to evaluate the accuracy of each damping model. We examine whether the frequency-dependence of damping models like Rayleigh Mass may, in fact, offer advantages over conventional frequency-independent formulations. We also evaluate the computational efficiency of each damping formulation.

2 SITE DESCRIPTION AND EMPIRICAL TRANSFER FUNCTIONS

The Delaney Park downhole array is situated in downtown Anchorage, Alaska. The soil profile at the downhole array (Figure 1a) features approximately 10 to 15 m of glacial outwash underlain by 30 m of Bootlegger Cove Clay, followed by glacial till. Strong-motion sensors at DPDA are installed at depths of 0, 4.6, 10.7, 18.3, 30.5, 45.4, and 61 m. However, for this study, only the 0 m and 61 m sensors were used to assess site response predictions, which are shown in Figure 1a. A Vs profile (Figure 1a) from Thornley et al. (2019) and 108 H/V measurements around the downhole array served as the backbone for developing a pseudo-3D Vs model using the H/V geostatistical method. This model (Figure 1b) spans 1.6 km × 1.6 km laterally and extends to 80 m depth.

In order to examine the accuracy of GRAs, ETFs between the borehole sensor at 60m and the surface sensor were computed using 56 low-amplitude recordings from the north–south and east–west components of 28 events, with PGAs between 0.001 and 0.01 g, magnitudes from 3.0 to 5.1, and source-to-site distances ranging from 10 to 96 km. The representative ETF in this study is defined as the lognormal median (LM_{ETF}) of the individual ETFs calculated for each ground motion, as shown in Figure 1c. Variability was quantified by computing the natural logarithmic standard deviation ($\sigma_{ln,\,ETF}$) at each frequency. The fundamental-, 1st-, 2nd-, and 3rd-higher mode peaks (f_0, f_1, f_2, and f_3, respectively) of the ETF are indicated in Figure 1c.

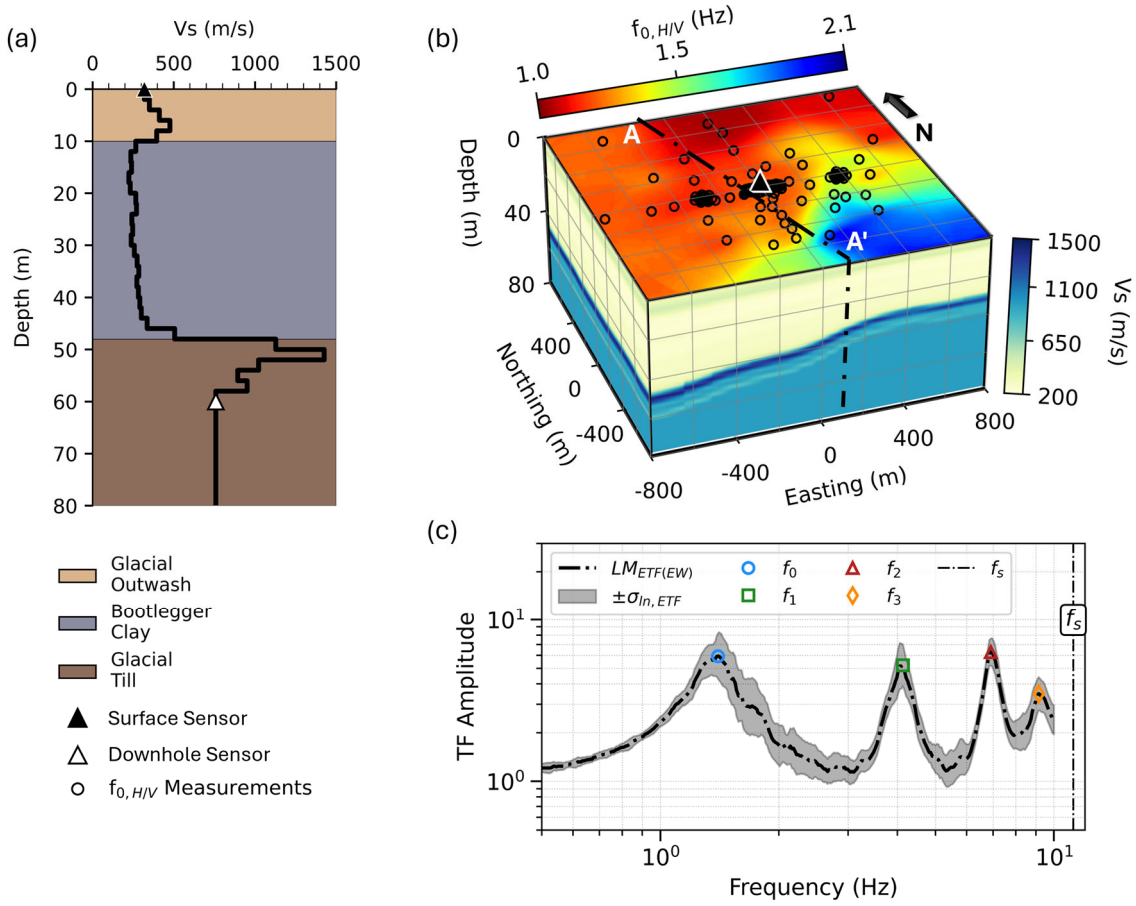

Figure 1: (a) 1D Vs profile from Thornley et. al (2019) and soil layers at the DPDA site, (b) pseudo-3D Vs model of the DPDA site developed using the H/V geostatistical approach, and (c) the lognormal median ETF (LM_{ETF}) along with the ± standard deviation ($\sigma_{ln,\,ETF}$) band computed from 56 small strain ground motions recorded at DPDA. Also indicated in (c) are the fundamental mode (f_0), 1st higher mode (f_1), 2nd higher mode (f_2), and 3rd higher mode (f_3) peaks of the ETF, along with the maximum resolvable frequency (f_s) based on numerical model descritization.

3 DESCRIPTION OF THE NUMERICAL MODEL

To capture the frequencies beyond the 3rd-higher mode peak in the ETF, the pseudo-3D model was discretized into 2-m cubical cells. This allowed a maximum frequency resolution (f_s) of 11.2 Hz based on 10 elements per shortest propagating wavelength, with the softest soil layer at DPDA having a Vs of 224 m/s. This resulted in a total of 25.6 million elements after discretization. Given the large number of elements and the need to perform numerous GRAs with different damping formulations, 3D GRAs were not feasible for this study. As a practical alternative, 2D GRAs were performed using the cross-section that best captured the spatial heterogeneity at the DPDA site. To make this determination, cross-sections were extracted at 15° azimuthal intervals and the degree of heterogeneity was evaluated using the coefficient of variation (COV) in Vs. The cross-section at 165° azimuth exhibited the highest COV (0.24) and was therefore identified as the most heterogeneous. This cross-section, denoted as AA' in Figure 1b, is illustrated in Figure 2a.

In addition to Vs, other material properties input into the numerical model include mass density, Poisson's ratio and damping ratio. A constant mass density of 2000 kg/m³ was assumed for all zones. Poisson's ratio was set at 0.30 for dry soil zones, 0.48 for saturated zones below the water table (assumed at 20 m), and 0.30 for rock-like materials with Vs greater than 760 m/s. D_{min} values were computed using the empirical method by Darendeli (2001), incorporating input parameters such as plasticity index, overconsolidation ratio, and effective confining stress. For the calculation of D_{min}, an excitation frequency of 3 Hz was used to better represent the energy distribution of the input motion across the dominant frequency range for DPDA (1-10 Hz), as indicated by the ETF (refer to Figure 1c).

While conventional analyses typically rely on D_{min}, this study also implemented an inflated damping ratio ($8 \times D_{min}$). This increased damping value was derived by calibrating the analytical 1D TTF to match the amplitude of the fundamental peak of the ETF at DPDA, similar to the approach documented in Tao and Rathje (2019). The multiplier is meant to account for scattering effects and other attenuation mechanisms not explicitly captured in 1D site response. However, as shown below, it also helps to improve multi-dimensional site response.

The small-strain 1D damping profiles were used as baselines for developing a pseudo-3D damping model for DPDA following the same procedure used for developing the pseudo-3D Vs model. From this pseudo-3D damping model, the 2D damping cross-section corresponding to the most heterogeneous Vs cross-section (Azimuth 165°) was extracted, as shown in Figure 2b. The damping formulations employed in this study are described in the following section.

To ensure consistent input energy distribution across the frequency range of interest, combined Ricker wavelets with sufficient energy between 1.0 and 10 Hz were used as broadband input motions. Quiet boundary conditions were used at the base and free-field boundaries were applied at the sides to avoid reflection of waves back into the model. Although free-field boundaries were employed to absorb outgoing seismic waves, the cross-section was extended to an additional 200m on each side to further reduce residual wave reflections.

4 DAMPING FORMULATIONS

Three damping formulations were implemented within the FLAC-3D framework to explore their effects on wave attenuation and site response prediction:

4.1 *Full Rayleigh Damping*

This conventional formulation combines mass- and stiffness-proportional terms (α and β, respectively), resulting in a damping matrix expressed as a combination of the mass and stiffness matrices of the system. In practice, it is often used as a tunable formulation by adjusting α and β to approximate a target damping ratio over a desired frequency range. In this study, the damping curve was fitted across the desired frequency range to a target damping value using root mean square (RMS) minimization, optimizing the fit between the half-amplitude bandwidth before the fundamental mode peak and the half-amplitude bandwidth after the third-higher mode peak.

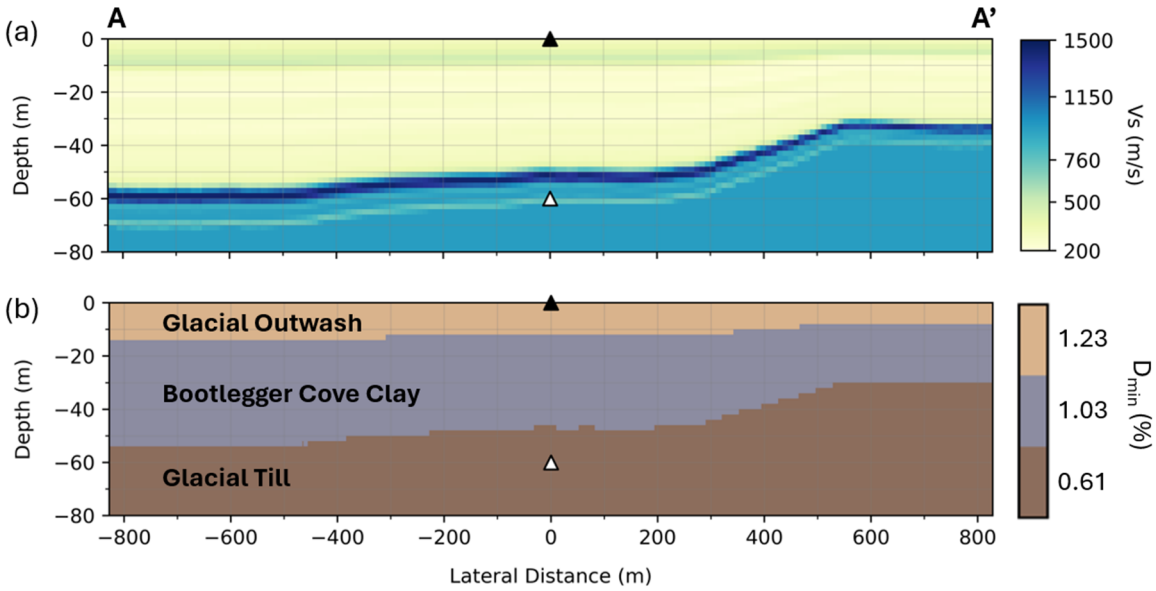

Figure 2: (a) Vs, and (b) Small-strain damping ratio (D_{min}) profile extracted along the most heterogeneous cross-section (Azimuth 165°) from the pseudo-3D Vs and damping models, respectively. Solid and hollow triangles denote the location of the surface and downhole sensors at DPDA, respectively.

4.2 *Maxwell Damping*

This formulation employs viscoelastic Maxwell elements, which are dashpot-spring assemblies in series, to provide a nearly constant damping ratio across a wide frequency range. As implemented in FLAC-3D, a three-element Maxwell model is used to achieve this behavior. Due to its relative insensitivity to frequency, Maxwell damping is sometimes also called "frequency-independent" damping. For further information on Maxwell damping and its implementation in FLAC-3D, readers are referred to Dawson & Cheng (2021).

4.3 *Rayleigh Mass Damping*

In FLAC-3D, the mass-proportional term of Full Rayleigh damping can be applied independently, which is referred to as Rayleigh Mass damping in this study. Rayleigh Mass damping is inherently frequency dependent, with higher damping at low frequencies and lower damping at higher frequencies. Although rarely used in site response analysis and lacking strong theoretical justification, this approach was adopted in the current study due to its empirical effectiveness. As demonstrated in the results, it provided the best agreement with observed site response while also offering computational efficiency.

5 GRA RESULTS AND DISCUSSION

A total of six 2D GRAs were conducted in this study, comprising three damping formulations (Full Rayleigh, Maxwell, and Rayleigh Mass damping) and two small-strain damping ratios (D_{min} and $8\times D_{min}$). TTFs were computed as the ratio of the Fourier Amplitude Spectra (FAS) of the simulated motion at the surface and downhole recordings. All FAS were smoothed using Konno & Ohmachi (1998) with a b-value of 75 to maintain consistency with ETFs. Two different 1D TTFs, using damping ratios of D_{min} and $8\times D_{min}$, were also computed using the closed-form, analytical solution. Finally, these total of eight cases (six 2D TTFs and two 1D TTFs) were compared against the recorded median ETF to assess site response predictions (Figure 3). Comparisons were made in terms of qualitative and quantitative measures. For quantitative comparison, the Pearson coefficient (r) and transfer function misfit (m_{TF}) were used. For details regarding r and m_{TF}, readers are referred to Teague et al. (2018). Here, a higher r and a lower m_{TF} signify a better fit.

The 1D analytical TTFs (dashed and solid green lines in Figure 3) demonstrate the sensitivity of TTF amplitudes to damping. When using the conventional D_{min}, the 1D TTF significantly overestimated the amplitude at the fundamental and the first-higher mode peak. Applying a modified damping ratio ($8 \times D_{min}$) improved alignment with the ETF at the fundamental peak but resulted in substantial underprediction of higher mode amplifications. This behavior is visible in the reduced amplitude of subsequent peaks and the positive residuals in the lognormal residual plot (Figure 3b), indicating that increasing damping in 1D improved low-frequency agreement but suppressed higher-frequency content.

Among the 2D TTFs obtained using the D_{min} damping ratio, all three damping formulations showed improvements in predicting amplitudes compared to the 1D TTF with D_{min}, though their accuracy varied. The 2D Full Rayleigh damping case (dashed orange) overpredicted both the fundamental and first-higher mode peaks, as reflected in the large negative lognormal residuals around those frequencies. Maxwell damping (dashed blue) exhibited similar overpredictions but performed slightly worse at higher frequencies due to minor shifts in modal peaks. Rayleigh Mass damping (dashed red) produced predictions similar to Full Rayleigh damping at the fundamental and first-higher mode peaks but showed slightly better agreement at the second-higher mode peak, with residuals closer to zero around 7 Hz. Quantitative comparison showed that, between 2D GRA TTFs obtained using D_{min}, the differences in predictive accuracy were minor, as illustrated in Figures 3c and 3d. The Pearson correlation coefficient (r), shown in Figure 3c, was lowest for Maxwell damping (D_{min}) and highest for Rayleigh Mass damping (D_{min}), although the differences were small. The TTF misfit metric (m_{TF}), shown in Figure 3d, was greatest for Maxwell damping, largely due to frequency shifts, while Rayleigh Mass damping exhibited the lowest misfit among D_{min} cases.

When the damping ratio was increased to $8 \times D_{min}$, the 2D GRA TTFs obtained using Full Rayleigh damping (solid orange) closely matched the fundamental peak but severely overdamped the higher modes, with residuals approaching 2 near the second-higher mode frequency (Figure 3b). With the increased damping ratio, Maxwell damping (solid blue) not only overdamped the higher modes significantly, but also introduced noticeable shifts in frequency content. This resulted in even higher residuals than those observed with Full Rayleigh damping. In contrast, Rayleigh Mass damping with $8 \times D_{min}$ (solid red) achieved the best agreement across the entire frequency range. It more accurately matched the amplitude and frequency of both the fundamental and higher mode peaks compared to the other two formulations, with lognormal residuals remaining close to zero. Unlike the 2D GRAs conducted using the D_{min} damping ratio, the 2D GRAs performed using $8 \times D_{min}$ showed pronounced differences between damping formulations. Maxwell damping combined with $8 \times D_{min}$ yielded the lowest r and the highest m_{TF} of all eight cases. In contrast, Rayleigh Mass damping produced the highest r and the lowest m_{TF}, confirming its superior overall performance.

Beyond accuracy, computational efficiency is a critical consideration in large-scale ground response analyses. To evaluate this aspect, the runtime required to complete a 10-second simulation using an AMD Threadripper pro 5995WX processor with 64 cores, and a timestep equal to the critical timetep for each case, was recorded for each damping formulation and damping ratio. These results are summarized in Table 1.

Table 1: Analysis Runtime

Damping Formulation	Damping Ratio	Analysis Runtime
Full Rayleigh	$1 \times D_{min}$	09 min 19 sec
Full Rayleigh	$8 \times D_{min}$	51 min 45 sec
Maxwell	$1 \times D_{min}$	04 min 19 sec
Maxwell	$8 \times D_{min}$	06 min 30 sec
Rayleigh Mass	$1 \times D_{min}$	03 min 34 sec
Rayleigh Mass	$8 \times D_{min}$	03 min 41 sec

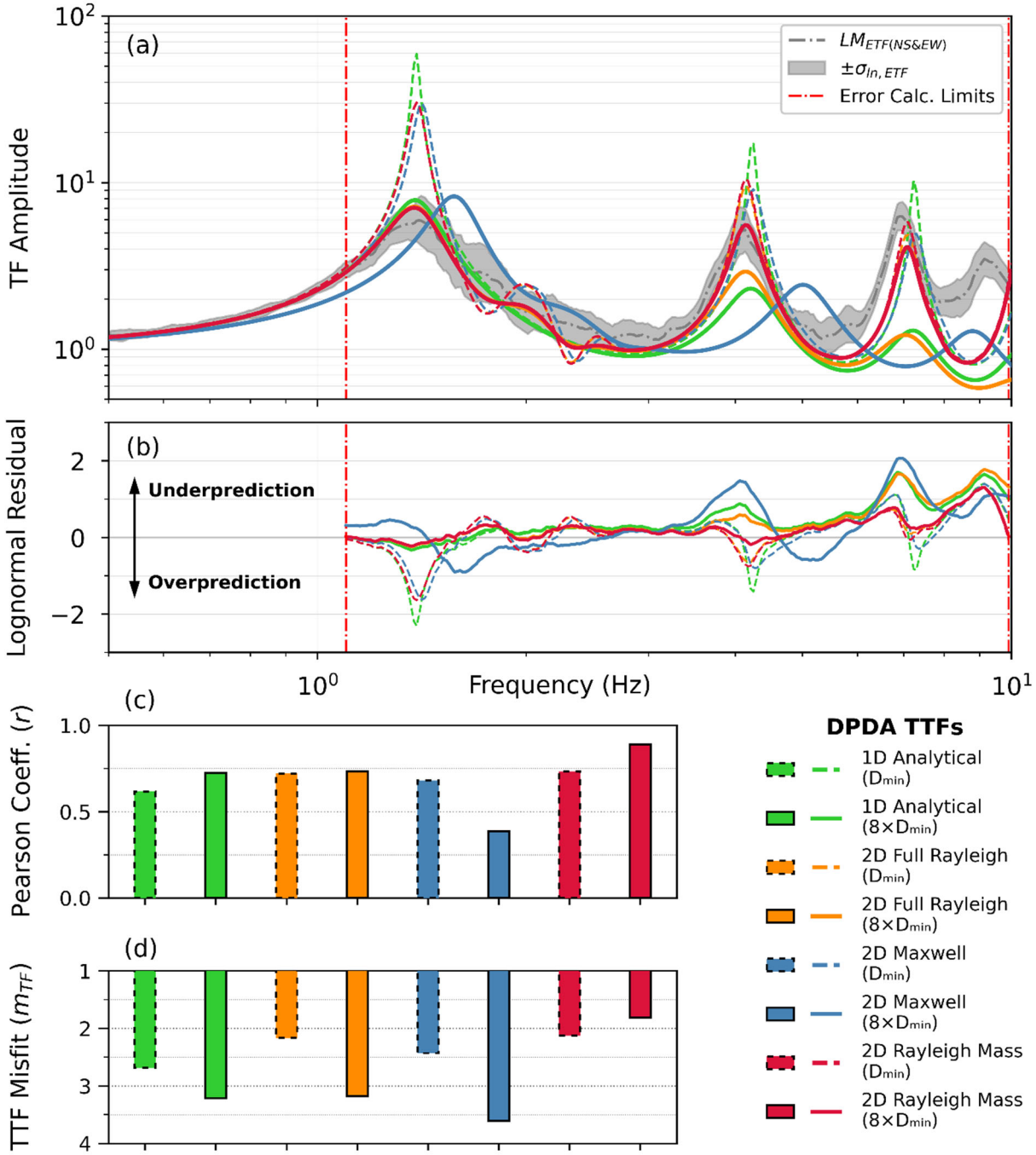

Figure 3: Site response predictions from eight GRA cases at the DPDA site using different damping formulations and damping ratios. Shown are: (a) comparison between simulated TTFs and the ETF, (b) lognormal residuals between the TTFs and ETF showing under/over prediction across frequencies, (c) Pearson correlation coefficient, and (d) TTF misfit associated with each case.

As shown in Table 1, Rayleigh Mass damping was the most computationally efficient, with runtimes under 4 minutes for both damping ratios. Maxwell damping required moderately more time, while Full Rayleigh damping required significantly more time, especially for the $8 \times D_{min}$ case, which took over 50 minutes. These findings underscore the practical advantage of Rayleigh Mass damping in reducing simulation time, an advantage that becomes even more critical when scaling up to full 3D ground response analyses.

These findings indicate that although increasing damping improved low-frequency predictions across all cases, Rayleigh Mass damping provided the best agreement across the full frequency spectrum. In addition to its accuracy, it also demonstrated the highest computational efficiency, making it a practical and effective solution for 2D GRA at the DPDA site.

6 CONCLUSION

This study evaluated the influence of three damping formulations and two small-strain damping ratios on 2D ground response analysis at the DPDA site. Increasing the small-strain damping ratio improved agreement with the ETF at the fundamental frequency but resulted in underprediction of higher mode peaks for both Full Rayleigh and Maxwell damping. Rayleigh Mass damping combined with $8 \times D_{min}$ achieved the best overall agreement with the ETF across the full

frequency range. It also had the shortest computation time, making it both accurate and efficient for practical applications.

Notably, the two frequency-independent formulations, Full Rayleigh and Maxwell damping, were less successful in replicating the amplitude of the observed site response, particularly at higher mode frequencies which were significantly over-damped. This highlights a critical insight: strict adherence to frequency-independent damping assumptions may not always yield the most realistic or reliable results. The superior performance of Rayleigh Mass damping, despite its theoretical limitations and inherent frequency dependence, challenges the long-held belief that damping must be modeled as frequency-independent to accurately capture site response. Given the incomplete understanding of wave attenuation mechanisms like wave scattering in geomaterials, these findings underscore the need to reevaluate conventional damping strategies. At the present, damping formulations should be treated as pragmatic, tunable approximations rather than precise physical models. Within this context, Rayleigh Mass damping emerges as a practical and effective option for simulating complex, laterally varying sites like DPDA. These results should be corroborated at other downhole array sites.

7 ACKNOWLEDGEMENTS

The H/V data at DPDA were collected with funding from Pacific Gas and Electric (PG&E). Any opinions, findings, or recommendations expressed in this article are those of the authors and do not necessarily reflect the views of PG&E..

8 REFERENCES

Afshari, K., & Stewart, J. P. (2019). Insights from california vertical arrays on the effectiveness of ground response analysis with alternative damping models. *Bulletin of the Seismological Society of America*, *109*(4), 1250–1264. https://doi.org/10.1785/0120180292

Darendeli, M. Baris. (2001). *Development of a new family of normalized modulus reduction and material damping curves* [Ph.D. Dissertation]. University of Texas at Austin.

Dawadi, N., Hallal, M. M., & Cox, B. R. (2024). Two-dimensional Ground Response Analyses at the Delaney Park Downhole Array Site. *Japanese Geotechnical Society Special Publication*, *10*(9), 207–212. https://doi.org/10.3208/jgssp.v10.ss-3-01

Dawadi, N., Jackson, T. S., & Cox, B. R. (2026). Three-Dimensional Ground Response Analyses at the I-15 Downhole Array Site near Salt Lake City. *Geo-Congress*.

Dawson, E. M., & Cheng, Z. (2021). *Maxwell Damping: An Alternative to Rayleigh Damping*. *2011*, 34–45. https://doi.org/10.1061/9780784483701.004

Hallal, M. M., & Cox, B. R. (2021a). An H/V geostatistical approach for building pseudo-3D Vs models to account for spatial variability in ground response analyses Part I: Model development. *Earthquake Spectra*, *37*(3), 2013–2040. https://doi.org/10.1177/8755293020981989

Hallal, M. M., & Cox, B. R. (2021b). An H/V geostatistical approach for building pseudo-3D Vs models to account for spatial variability in ground response analyses Part II: Application to 1D analyses at two downhole array sites. *Earthquake Spectra*, *37*(3), 1931–1954. https://doi.org/10.1177/8755293020981982

Hallal, M. M., & Cox, B. R. (2023). What Spatial Area Influences Seismic Site Response: Insights Gained from Multiazimuthal 2D Ground Response Analyses at the Treasure Island Downhole Array. *Journal of Geotechnical and Geoenvironmental Engineering*, *149*(1). https://doi.org/10.1061/jggefk.gteng-11023

Hallal, M. M., Cox, B. R., & Vantassel, J. P. (2022). Comparison of State-of-the-Art Approaches Used to Account for Spatial Variability in 1D Ground Response Analyses. *Journal of Geotechnical and Geoenvironmental Engineering*, *148*(5). https://doi.org/10.1061/(asce)gt.1943-5606.0002774

Itasca Consulting Group, Inc. (2023). *FLAC3D — Fast Lagrangian Analysis of Continua in Three-Dimensions* (9.0).

Konno, K., & Ohmachi, T. (1998). Ground-motion characteristics estimated from spectral ratio between horizontal and vertical components of microtremor. *Bulletin of the Seismological Society of America*, *88*(1), 228–241. https://doi.org/10.1785/BSSA0880010228

Tao, Y., & Rathje, E. (2019). Insights into Modeling Small-Strain Site Response Derived from Downhole Array Data. *Journal of Geotechnical and Geoenvironmental Engineering*, *145*(7). https://doi.org/10.1061/(asce)gt.1943-5606.0002048

Teague, D. P., Cox, B. R., & Rathje, E. M. (2018). Measured vs. predicted site response at the Garner Valley Downhole Array considering shear wave velocity uncertainty from borehole and surface wave methods. *Soil Dynamics and Earthquake Engineering*, *113*, 339–355. https://doi.org/10.1016/j.soildyn.2018.05.031

Thornley, J., Dutta, U., Yang, Z. J., & Fahringer, P. (2019). In situ shear-wave velocity measurements at the Delaney Park Downhole Array, Anchorage, Alaska. *Seismological Research Letters*, *90*(1), 395–400. https://doi.org/10.1785/0220180178

Tsai, C.-C., & Hashash, Y. M. (2009). Learning of Dynamic Soil Behavior from Downhole Arrays. *Journal of Geotechnical and Geoenvironmental Engineering*, *135*(6), 745–757. https://doi.org/10.1061/(asce)gt.1943-5606.0000050